Temperature, surface roughness and anisotropy effects on the tangential momentum accomodation coefficient between Pt(100) AND Ar

T. Tung Pham, Quy-Dong To, Guy Lauriat, Céline Léonard, V. H. Vo

DRAFT μFLU12- MICROFLUIDICS2012/93

TEMPERATURE, SURFACE ROUGHNESS AND ANISOTROPY EFFECTS ON THE TANGENTIAL MOMENTUM ACCOMMODATION COEFFICIENT BETWEEN PT(100) AND AR

Thanh Tung Pham[1], Quy Dong To*[1], Guy Lauriat[1], Van Hoang Vo[2]
[1]Mailing address
thanh-tung.pham@univ-paris-est.fr, quy-dong.to@univ-paris-est.fr, guy.lauriat@univ-paris-est.fr
[2]Mailing address
vvhoang2002@yahoo.com

KEY WORDS

TMAC, molecular beaming method, molecular dynamics, random roughness, temperature effect, random atom deposition.

ABSTRACT

In this paper, we study the influence of Platinum (100) surface morphology on the Tangential Momentum Accommodation Coefficient (TMAC) with Argon using Molecular Dynamics method (MD). The coefficient is computed directly by beaming Ar atoms into the surfaces and measuring the relative momentum changes. The wall is maintained at a constant temperature and its interaction with the gas atoms is governed by the Kulginov potential [1]. To capture correctly the surface effect of the walls and atoms trajectory, the Quantum Sutton-Chen multi-body potential is employed between the Pt atoms [2]. Effects of wall surface morphology and incident direction, temperature are considered in this work and provide full information of gas-wall interaction.

1. Introduction

In most applications concerning a fluid flowing past a solid surface, the no-slip conditions are usually employed: the fluid velocity at the wall is assumed to be the same as the surface velocity. This assumption, which works very well in many practical problems, breaks down when the channel height in consideration is at micro/nano length scale ([3], for example.). In the framework of the kinetic theory of gases, Maxwell introduced a gas-wall interaction parameter, the Tangential Momentum Accommodation Coefficient (TMAC), to quantify the slip effects [4]. He postulated that after collision with the wall, a gas atom rebounds either diffusively or specularly, with the associated portions of TMAC and $1 - \mathrm{TMAC}$, respectively. The slip velocity, v_{slip}, equal to the difference between the gas velocity, v, at the wall and the wall velocity, v_{wall}, can be evaluated by the following expression

$$v - v_{wall} = v_{slip}, \quad v_{slip} = \left(\frac{2 - \mathrm{TMAC}}{\mathrm{TMAC}}\right) \lambda \frac{\partial v}{\partial n} \tag{1}$$

where λ is the mean free path and $\frac{\partial v}{\partial n}$ is the normal derivative of the gas velocity at the wall. Although Molecular Dynamics simulations showed that the reflection mechanism is more complicated than Maxwell's postulate, the coefficient TMAC is still widely used due to its simplicity. In practice, a fully accommodated coefficient, TMAC = 1, is frequently used whereas experiments record smaller values ranging from 0.7 to 1.0 and MD simulations results are even much smaller [5].

* Corresponding author

Table 1: Parameters of the Pt-Ar pairwise potential of Kulginov .

V_0 (eV)	α (Å^{-1})	R_0 (Å)	C_6 (eV.Å^6)
20000	3.3	-0.75	68.15

Based on Eq.(1), the TMAC parameter for a gas-wall couple can be determined by either experiments [6] or Molecular Dynamics [7, 8] in the Navier Stokes slip regime. However, most MD simulations of flows were done at nanoscale [9] and do not have the same conditions as in experiments. In order to compare TMAC calculations with measurements for dilute gases, a more relevant MD approach consists in studying every single gas-wall collision event. Consequently, TMAC can be computed directly by projecting gas atoms into the surfaces and finding momentum changes [10]. This approach, which is quite similar to beam experiments [11], provides insights into the reflection mechanism and can be used to improve the Maxwell's model incompleteness.

Generally, TMAC results obtained from MD simulations depend on the following factors:
- The interaction potential between the gas/wall atoms.
- The dimension of the simulation models. In general, 3D models are better than 2D since it accounts for interactions of the gas atom with all its neighbors including out of plane solid atoms.
- The potential between the solid atoms must be good enough to reproduce the free surface effect. It is well known that the distance between the atomic layers near the free surface are much smaller than in the bulk.
- The temperature effect must be considered as gas molecules are adsorbed easier at cold walls than at hot walls, which can results in a higher TMAC.
- The surfaces are not always ideally smooth and can have different morphology (e.g randomly rough or textured surfaces).

This work aims at including these features in simulations of molecular beam experiments. The gas/wall couple under consideration is Argon and Platinum. The paper is organized as follows. After the Introduction, Section 2 is devoted to the description of the computational method. It discusses briefly the choice of potentials, the method to prepare surface sample and MD simulation of gas/wall interaction. We remark that a part of surface sample preparation requires a separate molecular dynamics simulation of film deposition processes in order to create a realistic random roughness surface. The TMAC results issued from the calculations are then shown in Section 4. Finally, conclusions and perspectives are discussed.

2. Computation model

2.1 Interatomic potential

The interatomic potentials play an important part in the molecular dynamics simulations since they govern the dynamics of the system and, thus the accuracy of the results. In this work, the following van der Waals type pair potential between At and Pt derived by Kulginov et al. [1] is used

$$\phi_{Ar-Pt}(R_{Ar-Pt}) = V_0 e^{-\alpha(R_{Ar-Pt}-R_0)} - \frac{C_6}{R^6_{Ar-Pt}}, \quad R_{Ar-Pt} = |\mathbf{r}_{Ar} - \mathbf{r}_{Pt}| \tag{2}$$

where R_{Ar-Pt} is the distance between an Ar atom at location $\mathbf{r}_{Ar}$ and a Pt atom at location $\mathbf{r}_{Pt}$, or *vice versa*. The values of the potential parameters are given in Tab. 1. Contrary to usual Lennard-Jones potentials, the repulsive part of this pair potential has a Born-Mayer form and provides a better description of the strong repulsion of the electrons. The pairwise potential parameters have been empirically adjusted such that the laterally average potential reproduces the measured properties of an Ar atom adsorbed on a slab of Pt atoms, i.e. a well depth of about 80 meV [12] and, a vibrational frequency of the adsorbed atom of about 5 meV [13]. The van der Waals interaction of an Ar atom with a platinum surface can be evaluated from the Ar-polarizability and the Pt-dielectric function.

In terms of the potential between the Pt atoms, the multi-body Quantum-Sutton Chen (QSC) potential is used [14]. As a particular Finnis-Sinclair potential type, the QSC potential includes quantum corrections and predict

Table 2: Quantum Sutton-Chen parameters for Pt.

n	m	ϵ (eV)	c	a (Å)
11	7	9.7894e-3	71.336	3.9163

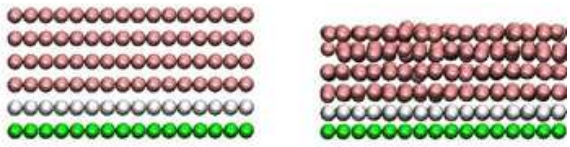

Figure 1: Surface effects: the fully relaxed configuration (right) is different from initial configuration (left). The solid film system is composed of fixed atoms (green), thermostat atom (white) and normal atoms (red).

better temperature dependent properties. For a system of N Pt-atoms, the potential is given by the following expression

$$E_{pot,Pt} = \epsilon \left[\frac{1}{2} \sum_{i=1}^{N} \sum_{\substack{j=1 \\ j \neq i}}^{N} \left(\frac{a}{r_{ij}} \right)^n - c \sum_{i=1}^{N} \rho_i^{1/2} \right], \quad \rho_i = \sum_{\substack{j=1 \\ j \neq i}}^{N} \left(\frac{a}{r_{ij}} \right)^m \tag{3}$$

where a is the lattice constant, R_{ij} the distance between atom i and j and the local density ρ_i of atom i. The parameters ϵ and a determine the scales of energy and length, respectively and, n and m the range and shape of the potential. These potential parameters are given in Tab. 2. Combining the two potentials, we can compute the total potential of the system

$$E_{pot} = \sum_{i=1}^{N} \phi_{Ar-Pt}(R_{Ar-i}) + E_{pot,Pt} \tag{4}$$

and the force $\mathbf{f}_i$ acting on atom i at position $\mathbf{r}_i$ by

$$\mathbf{f}_i = -\frac{\partial E_{pot}}{\partial \mathbf{r}_i} \tag{5}$$

Since we only consider the interaction of one Ar atom with a Pt surface, there is no contribution of the Ar-Ar term in the total potential formula E_{pot}. The accuracy of the QSC potential for Pt has been justified by Subramanian et al. [2] as it allow to correctly reproduce the melting temperature and the specific heats of the material. Although its implementation is more costly than the harmonic (spring) potential, it should better reproduce the surface effects, since atoms near the free surfaces are different from the bulk. Our tests on the QSC potential show that in fully relaxed equilibrium system, the interatomic distance near the free surfaces is much smaller than in the bulk (see Fig. 1). As shown by Arya et al. [15], the lattice constant parameter can have significant impact on TMAC.

2.2 Surface samples

In this paper, three types of surfaces are considered: smooth surfaces, periodically patterned surfaces and randomly rough surfaces. The orientation of their free surfaces is (100) according to the Miller index. Initially, the Pt atoms are arranged in layers and the two lowest ones (phantom atoms) are used to fix the system and for thermostat purpose. The remaining Pt atoms are free to interact with other solid atoms and gas atoms. The random arrangement of these atoms defines the "rough" state of the surface and will be detailed later on.

A smooth surface model is a system composed of 768 atoms arranged in 6 layers, all of which are in perfect crystal order. The nanotextured models are constructed from the smooth surface model by adding successively atom layers to create pyramids with the slope angle $45°$. The slope is necessary to assure the stability of the

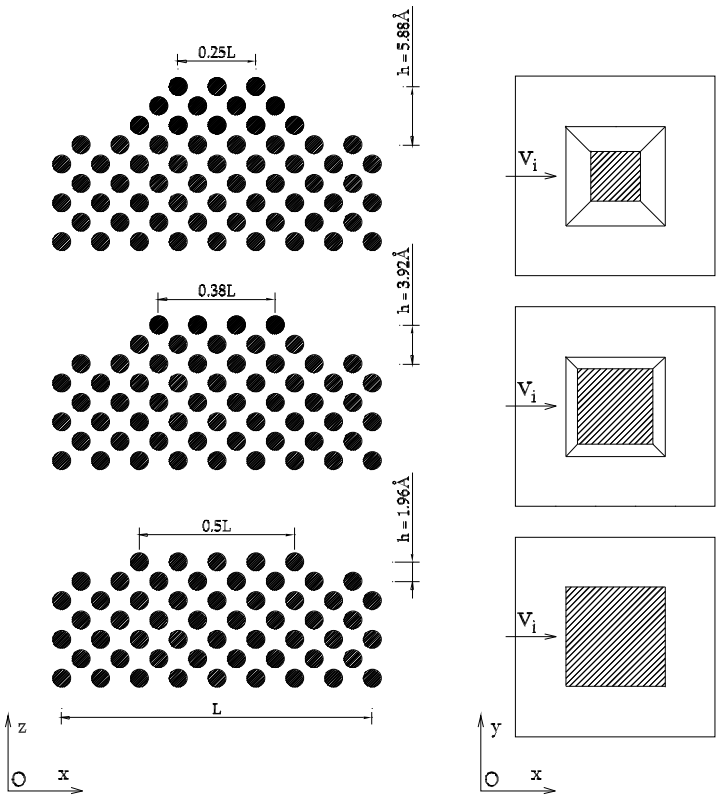

Figure 2: Nanotextured surface of type A (square)

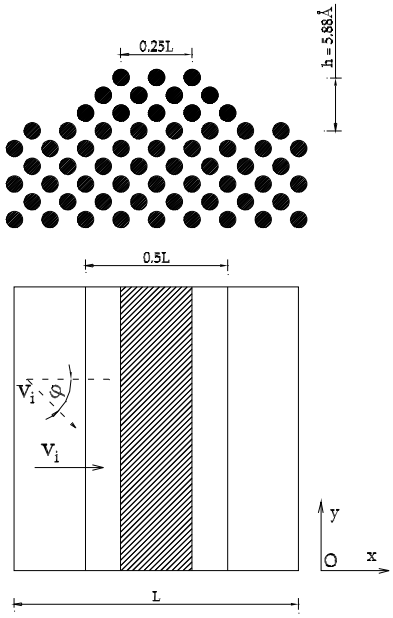

Figure 3: Nanotextured surface of type B (strip)

system since perfectly vertical blocks (slope angle 90°) are less stable: in many cases atoms migrate to lower positions and the blocks evolve into step-like structures with smaller potential energy. The base of the pyramid can be a square (type A, Fig. 2) or an infinite strip (type B, Fig. 3), so that both isotropic/anisotropic effect can be considered. Although these pyramids are simplified models of a real rough surface, it can show the dependence of TMAC on the roughness. The latter in MEMS/NEMS is reported to be several Å [3]. In this work, the highest peak, varying with the number of atoms layers added on the surfaces, ranges from 2 to 6 Å.

Randomly rough surface models are also constructed by adding atoms on the smooth surfaces in a random way. In the available literature, there are several mathematical models [16, 17, 18, 19] that describe random roughness. However, these models are not suitable at atomic scale: it is difficult to force atoms to be at given positions and, structure parameters such as orientation (100) and lattice constant must be respected. Furthermore such atomistic systems might not be appropriate in terms of potential energy. In our opinion, a randomly rough surface which is consistent with the internal atomistic structure, should be built from molecular dynamics simulations. Rapid cooling of thin films from the liquid state [20, 21] can create rough surfaces but the final systems could contain many defects (e.g. pores, dislocations) and non crystalline structure (e.g. polycrystal, amorphous). As the paper focuses on Pt (100), the rough surfaces are constructed by deposed atoms randomly on the existing smooth Platinum surface. Since this procedure is quite similar to the film vapor-deposition processes, it is asssumed that the created surface is quite close to real MEMS/NEMS surfaces. The procedure of the material deposition is described as follows.

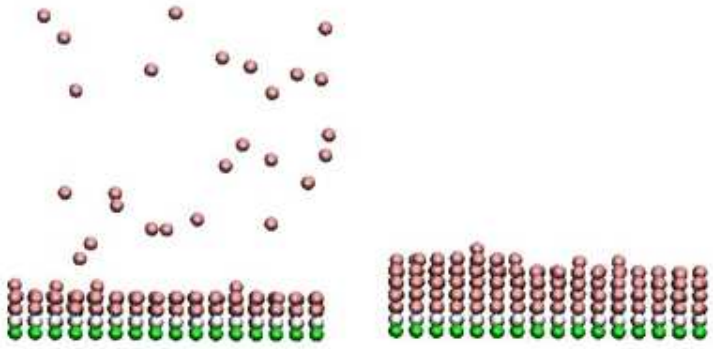

Figure 4: Snapshot of deposition process (left) and final thin film system (right)

The initial system is a Pt plate made of four layers of 512 solid atoms, arranged in (100) fcc order. First, the system relaxes towards the minimal potential energy configuration. Then, after 2000 time steps of 10 fs, a Pt atom is inserted randomly from a height of 10 Å with the initial thermal velocity corresponding to 1000 K. Under the attraction force (QSC potential) from the Pt plate, the deposed Pt atoms move downwards until they reach the plate which is maintained at 50 K. (see a snapshot of the deposition process in Fig.4). Finally, when all inserted Pt atoms are attached firmly into the Pt plate, the whole system undergoes the anneal process at the ambient temperature $T_a = 300$ K with a time step equal to 20 fs. During the whole simulation, the Leap-Frog Verlet integration scheme is employed and the temperature is kept constant by simple velocity scaling method.

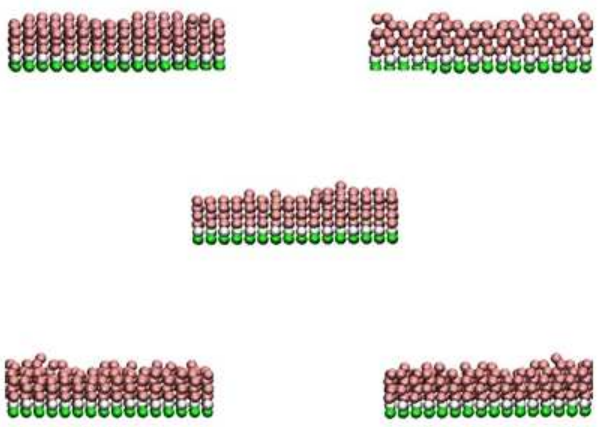

Figure 5: Five samples obtained from the deposition process

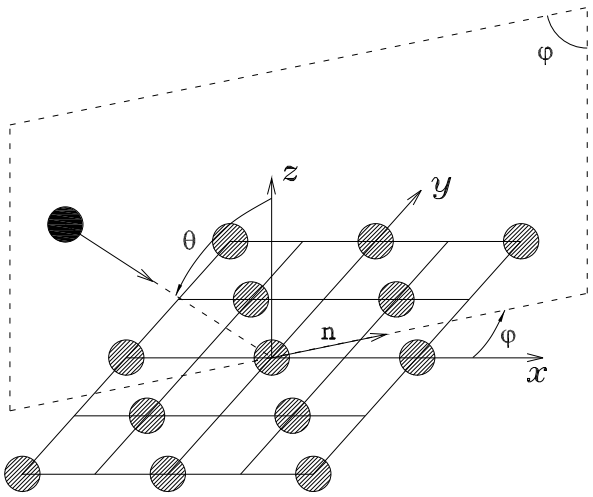

Figure 6: Representation of θ, φ in cartesian coordinate system

Figure 4 shows a snapshot of the final system whose total number of Pt atoms have reached 733. To improve the statistical results, 5 samples obtained thanks to the above described procedure are collected, as shown in Fig. 5.

2.3 Dynamics of gas/wall collision

In what follows, we describe the MD method used to simulate the gas-wall collision and to calculate the TMAC coefficient. The simulations were three dimensional: an Ar atom is projected into a Pt(100) surface with different incident angles θ and with different approaching φ-planes. In spherical coordinate system, (θ, φ) are the polar and azimuthal angles, respectively (see Fig 6). The *directional* TMAC_{dir} coefficient associated with each θ and φ is defined by the following formula [3]:

$$\text{TMAC}_{dir}(\theta, \varphi) = \frac{\langle v_{in} \rangle - \langle v_{rn} \rangle}{\langle v_{in} \rangle} \tag{6}$$

where v_{in} and v_{rn} are the projections of the incident and the reflected velocity on the vector $\mathbf{n}$, respectively. The latter is the intersection of the plane xOy and the φ-plane, i.e it lies on xOy and makes an angle φ with respect to Ox. Only one gas-wall collision is treated per simulation and the averages in Eq.(6) are taken over a large number of simulations (or collisions). The definition (6) is the most accurate description of gas-wall interaction since it is associated to every directions. We also calculate the *effective anisotropic* $\text{TMAC}_{an}(\varphi)$ coefficients using the same equation (6) but with gas atoms arriving from all directions: the direction of $\mathbf{v}_i$ is randomly uniform with $v_{in} > 0$. In the special case where the surface is isotropic, TMAC_{an} varies little with φ and a single *effective isotropic* TMAC_{iso} constant is sufficient to model gas-wall interaction as in Maxwell's model.
We assume first that an Ar atom only interacts with the Pt wall within a cutoff distance $r_c = 10$ Å. Since this distance is much smaller than the typical mean free path at atmospheric pressure or in high vacuum ($\lambda > 69$ nm), it can justify the choice of such a small region to calculate the TMAC coefficients. At the beginning of each simulation, an Ar atom is inserted randomly at the height r_c above the wall surface with initial incident velocity $\mathbf{v}_i$. The norm of $\mathbf{v}_i$ is equal to the thermal speed corresponding to the gas beam temperature T_g. Although the results of this work are obtained using a constant incident velocity corresponding to the gas temperature, we have done separate simulations using the Maxwell-Boltzmann velocity distribution and find that the TMAC is insensitive to this modification. A collision is considered as finished when the atom bounces back beyond the cutoff distance. Then the reflected velocity $\mathbf{v}_r$ is recorded for the statistical purpose and another Ar atom is reinserted randomly to continue the process. After approximatively 10000 collisions (simulations), converged values of TMAC values were obtained.

Throughout the simulations, periodic boundary conditions were applied along the x, y directions. The velocities and positions of gas atoms and the solid atoms at each time step are calculated by the usual Leap-Frog Verlet integration scheme. To control the temperature T_w of the system, the phantom technique is used: the Langevin

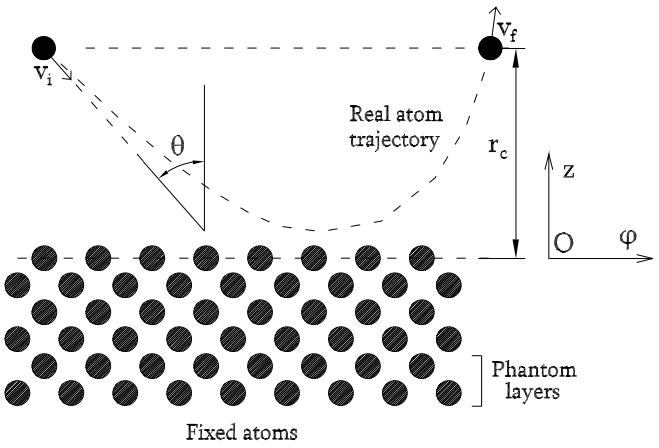

Figure 7: Molecular dynamics scheme. The incident argon atoms are with v_i velocities. θ is the incident angle. The Pt wall has a fcc structure with a (100) surface. The Pt atoms are controlled by Sutton-Chen potential.

thermostat [22] is applied to the atom layer above the fixed layers. The motion of an atom i belonging to this layer is governed by the equation

$$m_i \frac{d\mathbf{v}_i(t)}{dt} = -\xi \mathbf{v}_i(t) + \mathbf{f}_i(t) + \mathbf{R}_i(t). \tag{7}$$

In Eq.(7), $\mathbf{v}_i$ is the velocity of the atom i, $\mathbf{f}_i$ is the resulting force acting on it by the surrounding ones, m_i is the atomic mass and ξ is the damping coefficient. The third term $\mathbf{R}_i$ in the right hand side of Eq.(7) is the random force applied on the atom. In the simulation, it is sampled after every time step δt from a Gaussian distribution with zero average and mean deviation of $\sqrt{6\xi k_B T_w/\delta t}$. The simulations were carried out by setting time step and damping factor at the following values:

$$\delta t = 20 \text{ fs}, \quad \xi = 5.184 \times 10^{-12} \text{kg/s}. \tag{8}$$

The wall temperature T_w was kept at 200 K, 300 K and 400 K and the gas beam temperature T_g was kept at a slightly higher value than T_w, here $T_g = 1.1T_w$. Generally, to obtain the best statistical results, a typical run requires 4×10^7 time steps of 20 fs. All simulations were run on 9 processors, using a domain decomposition and the Message Passing Interface. The longest simulation takes about 20 CPU hours.

3. MD simulation results

3.1 Effects of temperature and roughness height

From the description of the models in Section 2, the coefficient TMAC$_{dir}$ can depend on the several input parameters: temperature, surface morphology, incident direction (θ, φ). The variation of TMAC$_{dir}$ in terms of these parameters is investigated in the following subsections.

The temperature effect on TMAC has been studied for confined fluid flows in a smooth nanochannel [8, 23] but, to our best knowledge, no work has been done by using 3D molecular beam simulations. The TMAC$_{dir}$ results at different temperatures are shown in Fig. 8. A general trend can be noticed here: the TMAC$_{dir}$ increases as the temperature decreases, ranging from 0.78 to 0.92 in the case of the highest roughness considered ($h = 5.88$ Å). This trend in TMAC$_{dir}$ variation can be explained by the fact that the adsorption is stronger with colder walls. Gas atoms stay longer near the wall, interact more with solid atoms and, as a result, the reflection is more diffusive. Similar remarks have been reported in [8, 23] for confined systems. For $h = 5.88$ Å and $T_w = 300\ K$,Tab. 3 shows that the TMAC$_{dir}$ value varies very little with the incident angle θ and very closed to the average isotropic value TMAC$_{iso} = 0.85$. This means that for this kind of surface, Maxwell's one parameter model is sufficiently accurate to model gas-wall interaction.
The TMAC$_{dir}$ coefficient increases with the roughness of the wall surface. Computations carried out for pyramidal structures at the temperature of 300 K show that the TMAC$_{dir}$ coefficient can reach up to 0.85 for

Table 3: TMAC_{iso} and $\mathrm{TMAC}_{dir}(\theta, \varphi)$ computed at $T_w = 300\ K$.

Surface type	φ	θ	TMAC_{dir}	TMAC_{iso}
A (h =5.88 Å)	0°	10°	0.87	–
	0°	30°	0.86	–
	0°	45°	0.85	–
	0°	60°	0.85	–
	0°	80°	0.83	–
	–	–	–	0.85
Random	0°	45°	0.92	
	–	–	–	0.92

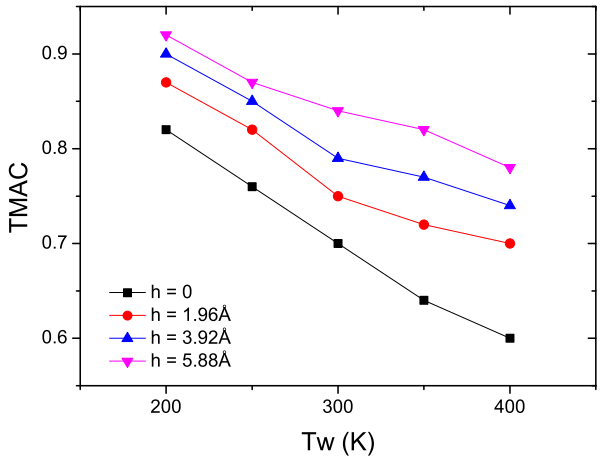

Figure 8: TMAC_{dir} computed for the wall of type A (square) at $T_w = 200\ K$, $250\ K$, $300\ K$, $350\ K$ and $400\ K$ for three roughness heights h with $\theta = 45°$ and $\varphi = 0°$.

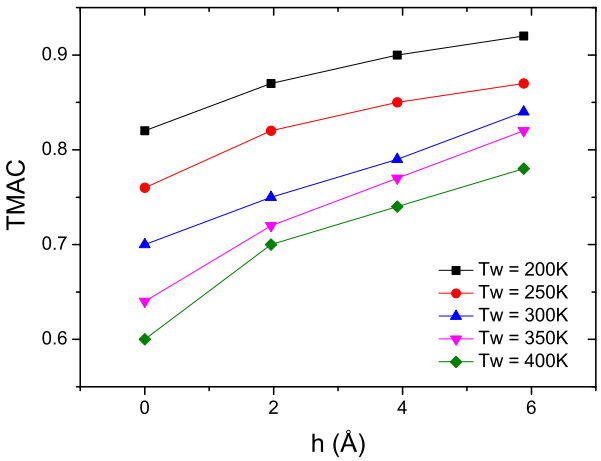

Figure 9: TMAC_{dir} computed for the wall of type A (square) with different roughness heights at $T_w = 200\ K$, $250\ K$, $300\ K$, $350\ K$ and $400\ K$ with $\theta = 45°$ and $\varphi = 0°$.

surfaces with the highest peak configuration (Fig. 8). It is clear that the presence of peaks leads to non uniform surface potentials with local minima where gas molecules can easily be trapped: the gas atoms adhere stronger

to the wall and lose their initial momentum. Moreover, the changes in local slopes produce more or less random variations in the local incident and reflection angles.
Next we considered the case of random surfaces obtained from the atom deposition process. With the same parameters for the deposition process, the TMAC_{dir} obtained for the five samples shown in Fig. 5 exhibit small differences, from 0.90 to 0.93 and is very closed the average isotropic value 0.92(see Table 3). Thus, in addition to the roughness height, the in-plane random arrangement of the atoms also plays a significant role on the accommodation coefficient.

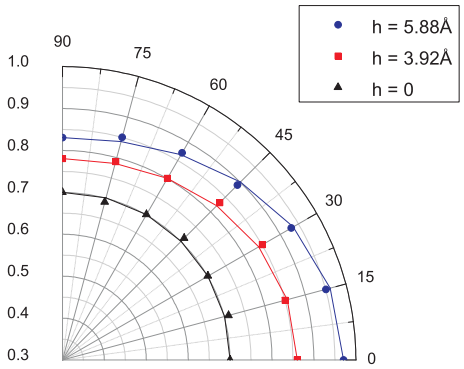

Figure 10: TMAC_{dir} computed for type-B walls (strip) versus azimuth angle φ for different roughnesses ($T_w = 300K$, $\theta = 45°$). The solid line is the analytical expression (9) used to fit numerical results.

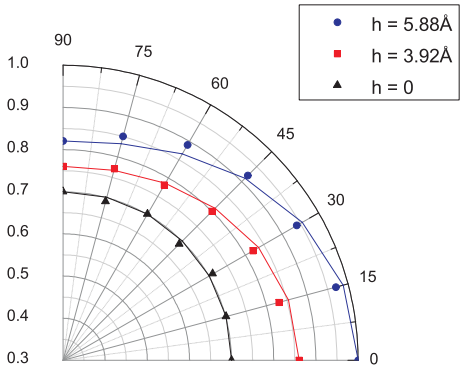

Figure 11: TMAC_{an} computed for type-B walls (strip) versus azimuth angle for different roughnesses ($T_w = 300K$). The solid line is the analytical expression (9) used to fit numerical results .

3.2 Surface anisotropy effect

An anisotropic wall surface can obstruct or facilitate the flows differently along different directions. Bazant and Vinogradova generalized Navier slip boundary conditions for anisotropic texture surface by using a tensorial slip length [24]. In the framework of kinetic theory, Dadzie and Meolans proposed a new scattering kernel that accounts for surface anisotropy [25]. Their formulation is based on three independent accommodation coefficients $\alpha_x, \alpha_y, \alpha_z$ along the three directions x, y, z. The coefficients α_x, α_y represent the tangential accommodation coefficients and α_z is the normal accommodation coefficient. The tangential accommodation coefficient α_n in direction n is then computed by the expression (see Appendix A)

$$\alpha_n = \alpha_x \cos^2 \varphi + \alpha_y \sin^2 \varphi \tag{9}$$

In this subsection, we study the anisotropy effect using MD and the directional TMAC definition in Eq.(6) and examine the relation (9). The anisotropy effect can be seen from Fig. 11: the TMAC_{dir} variation with φ is non uniform for rough surfaces. The accommodation process along the two directions x, y is highly different. The TMAC_{dir} is minimum when the atoms are projected along the longitudinal direction of the strip ($\varphi =$

$90°$), since the surface may be considered as almost smooth in that direction (see Fig. 3). This TMAC value correspond to α_y in the model of Dadzie and Meolans. The maximal TMAC values recorded for $\varphi = 0°$ and $h > 0$ can be attributed to the largest roughness effect in that direction and correspond to α_x in the model of Dadzie and Meolans. Moreover, Figures (10, 11) show a larger anisotropy effect for rough surfaces: the difference between the highest and the smallest TMAC value increases with the roughness height whereas the TMAC results depend very little on the beaming direction for a smooth surface. This could be explained by the fact that the smooth surface is isotropic. Although Figures 10, 11 show discrepancies of TMAC obtained in different ways, all curves can fit reasonably well the analytical relation (9).

4. Conclusions and perspectives

In this paper, we have studied the effects of temperature, surface roughness and anisotropy on the TMAC coefficient. The computation model is based on the molecular beam experiments and constructed with the accurate available potentials and interaction models. Although TMAC is not a simply gas/wall constant, the MD result range agrees quite well with the experimental range at the ambient temperature. The random roughness surface obtained from the atomic deposition simulation is also investigated in the paper.
Concerning the anisotropy effect, initial results on systems with strips show that TMAC varies with orientation. This provides insights and improvements to the Maxwell model which only account for isotropic effects.

5. Appendix - Anisotropic scattering kernel

For gas-wall interaction, Dadzie and Meolans [25] proposed an anisotropic scattering kernel $B(\mathbf{v}', \mathbf{v})$ defined by

$$B(\mathbf{v}', \mathbf{v}) = \sum_k \mu_k B_k(\mathbf{v}', \mathbf{v}) \tag{10}$$

in which

$$\begin{aligned} &\mu_{ij} = \alpha_i\alpha_j(1-\alpha_k), \quad \mu_i = \alpha_i(1-\alpha_j)(1-\alpha_k), \quad \mu_{ijk} = \alpha_i\alpha_j\alpha_k, \\ &\mu_0 = (1-\alpha_i)(1-\alpha_j)(1-\alpha_k), \quad i,j,k = x,y,z, \quad i \neq j \neq k \neq i. \end{aligned} \tag{11}$$

The vectors $\mathbf{v}', \mathbf{v}$ are respectively the arriving velocity and the reflected one and the constants $\alpha_x, \alpha_y, \alpha_z$ are the accommodation coefficients along the directions x, y, z. The elementary kernels B_k are given by the following expressions

$$\begin{aligned} B_0(\mathbf{v}', \mathbf{v}) &= \delta(v_z + v_z')\delta(v_x - v_x')\delta(v_y - v_y') \\ B_{xy}(\mathbf{v}', \mathbf{v}) &= \frac{1}{\pi C_w^2}\delta(v_z + v_z')e^{-(v_y^2+v_x^2)/C_w^2} \\ B_{iz}(\mathbf{v}', \mathbf{v}) &= \frac{2}{\sqrt{\pi}C_w^3}v_z\delta(v_j - v_j')e^{-(v_i^2+v_z^2)/C_w^2} \\ B_{xyz}(\mathbf{v}', \mathbf{v}) &= \frac{2}{\pi C_w^4}v_z e^{-(v_x^2+v_y^2+v_z^2)/C_w^2} \\ B_i(\mathbf{v}', \mathbf{v}) &= \frac{1}{\sqrt{\pi}C_w}\delta(v_z + v_z')\delta(v_j - v_j')e^{-v_i^2/C_w^2} \\ B_z(\mathbf{v}', \mathbf{v}) &= \frac{2}{C_w^2}v_z\delta(v_i - v_i')\delta(v_j - v_j')e^{-v_z^2/C_w^2}, \quad i,j = x,y, \quad i \neq j. \end{aligned} \tag{12}$$

The boundary conditions for particle distribution function $f(\mathbf{v})$ is then defined by

$$v_z f(\mathbf{v}) = \int_{\Omega'} |v_z'| f(\mathbf{v}')B(\mathbf{v}', \mathbf{v})d\mathbf{v}', \quad \Omega' = \mathbb{R} \times \mathbb{R} \times \mathbb{R}^- \tag{13}$$

We use Φ_j^- and Φ_j^+ to denote the incoming flux at the wall of the momentum j component. Then

$$\Phi_j^- = \int_{\Omega'} m|v_z'|v_j' f^-(\mathbf{v}')d\mathbf{v}', \quad \Phi_j^+ = \int_{\Omega} m|v_z|v_j f^+(\mathbf{v})d\mathbf{v}, \quad \Omega' = \mathbb{R}\times\mathbb{R}\times\mathbb{R}^+. \tag{14}$$

with f^- and f^- being the velocity distribution associated with the incident molecules and for the reflected molecules. Dadzie and Meolans proved the following relation

$$\frac{\Phi_j^- - \Phi_j^+}{\Phi_j^-} = \alpha_j, \quad j = x, y, z. \tag{15}$$

Since their model is based on three parameters $\alpha_x, \alpha_y, \alpha_z$ defined along given directions of a given system of coordinate. We are interested in the accommodation coefficients in a arbitrary direction. We consider a family of direction $\mathbf{n}$ lying in the plane xOy and make an angle φ with Ox. Consequently, the n component of the flux is related to x, y components by

$$\Phi_n^\pm = \cos\varphi\Phi_x^\pm + \sin\varphi\Phi_y^\pm \tag{16}$$

Since α_x and α_y are accommodation coefficients, the following relations

$$\begin{aligned}\Phi_n^+ &= \cos\varphi\Phi_x^+ + \sin\varphi\Phi_y^+ = (1-\alpha_x)\cos\varphi\Phi_x^- + (1-\alpha_y)\sin\varphi\Phi_y^- \\ &= (1-\alpha_x)\cos^2\varphi\Phi_n^- + (1-\alpha_y)\sin^2\varphi\Phi_n^-\end{aligned} \tag{17}$$

allow us to compute the accommodation coefficient along any direction n as in (9).

REFERENCES AND CITATIONS

[1] Kulginov D, Persson M, Rettner CT, Bethune DS (1996) An empirical interaction potential for the Ar/Pt(111) system. J Phys Chem 100:7919–7927.

[2] Subramanian KRSS, Venkat RB, Babu J (2006) Molecular dynamics simulation study of the melting and structural evolution of bimetallic Pd-Pt nanowires. Phys Rev B 74:155441.

[3] Karniadakis G, Beskok A, Aluru N (2005) Microflows and nanoflows: Fundamentals and simulation. Springer, New York.

[4] Maxwell J (1879) On stresses in rarified gases arising from inequalities of temperature. Philos T Roy Soc A 170:231-256.

[5] Cao B, Sun J, Chen M, Guo Z (2009) Molecular momentum transport at fluid-solid interfaces in MEMS/NEMS: A Review. Int J Mol Sci 10:4638–4706.

[6] Arkilic E, Breuer K, Schmidt M (2001) Mass flow and tangential momentum accommodation in silicon micromachined channels. J Fluid Mech 437:29–43.

[7] To QD, Bercegeay C, Lauriat G, Leonard C, Bonnet G (2010) A slip model for micro/nano gas flows induced by body forces. Microfluid Nanofluid 8:417-422.

[8] Cao B, Chen M, Guo Z (2005) Temperature dependence of the tangential momentum accommodation coefficient for gases. Appl Phys Lett 86:091905.

[9] To QD, Pham TT, Lauriat G, Leonard C (2012) Molecular Dynamics Simulations of Pressure Driven Flows and Comparison with Acceleration Driven Flows. Advances in Mechanical Engineering (doi:10.155/2012/580763).

[10] Finger G, Kapat JS, Bhattacharya A (2007) Molecular dynamics simulation of adsorbent layer effect on tangential momentum accommodation coefficient. J Fluid Eng-T ASME 129:31-39.

[11] Rettner CT (1998) Thermal and tangential-momentum accommodation coefficients for N-2 colliding with surfaces of relevance to disk-drive air bearings derived from molecular beam scattering. IEEE T Magn 34:2387-2395.

[12] Head-Gordon M, Tully JC, Rettner CT, Mullins CB, Auerbach DJ (1991) On the nature of trapping and desorption at high surface temperatures. Theory and experiments for the Ar-Pt(111) system. J Chem Phys 94:1516–1527.

[13] Zeppenfeld P, Becher U, Kern K, David R, Comsa G (1990) Van Hove anomaly in the phonon dispersion of monolayer Ar/Pt(111). Phys Rev B 41:8549–8552.
[14] Sutton AP, Chen J (1990) Long-range Finnis-Sinclair potentials. Phil Mag Lett 61:139–146.
[15] Arya G, Chang HC, Maginn EJ (2003) Molecular simulations of knudsen wall-slip: effect of wall morphology. Mol Simulat 29:697–709.
[16] Bhushan B (2001) Modern Tribology Handbook. CRC Press, New York.
[17] Majumdar A, Bhushan B (1990) Role of fractal geometry in roughness characterization and contact mechanics of surfaces. J Tribol-T Asme 112:205–216.
[18] Mandelbrot BB (1982) The fractal geometry of nature. WH Freeman, New York.
[19] Mandelbrot BB, Passoja DE, Paullay AJ (1984) Fractal character of fracture surfaces of metals. Nature 308:1571–1572.
[20] Hoang VV, Dong TQ (2011) Free surface effects on thermodynamics and glass formation in simple monatomic supercooled liquids. Phys Rev B 84:174204.
[21] Dong TQ, Hoang VV, Lauriat G (2012) Molecular dynamics simulation of free standing amorphous nickel thin film (under preparation).
[22] Schlick T (2010) Molecular modeling and simulation: an interdisciplinary guide. Springer, New York.
[23] Spijker P, Markvoort AJ, Nedea SV, Hilbers PAJ (2010) Computation of accommodation coefficients and the use of velocity correlation profiles in molecular dynamics simulations. Phys Rev E 81:011203.
[24] Bazant M Z, Vinogradova O I (2008) Tensorial hydrodynamic slip 613:125–134.
[25] Dadzie SK, Meolans JG (2004). Anisotropic scattering kernel: Generalized and modified Maxwell boundary conditions. J Math Phys 45:1804–1819.
[26] Ramseyer C, Hoang PNM, Girardet C (1994) Interpretation of high-order commensurate phases for an argon monolayer adsorbed on Pt(111). Phys Rev B 49:2861–2868.